

Model for electron emission of high-Z radio-sensitizing nanoparticle irradiated by X-rays

R.Casta ^{*1}, J.-P.Champeaux¹, P.Cafarelli¹, P.Moretto-Capelle¹, and M.Sence¹

¹Laboratoire Collisions Agrégats Réactivité, IRSAMC, CNRS, UMR 5589, Université de Toulouse, UPS, F-31062 Toulouse, France.

June 17,2014

Abstract

In this paper we develop a new model for the electron emission of high-Z nanoparticle irradiated by X-rays. This study is motivated by the recent advances about the nanoparticle enhancement of cancer treatment by radiotherapy. Our original approach combines a pure probabilistic analytical model for the photon trajectories inside the nanoparticle and subsequent electron cascade trajectories based here on a Monte-Carlo simulation provided by the Livermore model implemented in Geant4. To compare the nanoparticle and the plane surface electron emissions, we also develop our model for a plane surface. Our model highlights and explains the existence of a nanoparticle optimal radius corresponding to a maximum of nanoparticle electron emission. It allows us to study precisely the nanoparticle photon absorption and electron cascade production depth in the nanoparticle.

1 Introduction

Electron emission by X-ray irradiated nanoparticle is an important subject of interest in the context of radiotherapy cancer treatment enhanced by nanoparticles of high-Z material such as gold. It has been shown that nanoparticles can improve cancer radiotherapy enhancing significantly cancer cell destruction [7, 11] and cancer healing on mice [10], comparatively to classical radiotherapy treatments. Few theoretical approaches are available concerning this improvement, for example hyperthermia [12, 19] or radical production [5] have been studied. One of them explains this increase of cancerous cells death by the nanoparticles emission of electrons. These electrons, released by the interaction of X-rays with nanoparticles, are supposed to be more efficient in the destruction of cancerous cells than the electrons released in water (or tissue) by the interaction of the same X-rays [3, 17, 4]. But this electron emission is not well known and consequently nanoparticle critical parameters such as size or composition are often chosen following others criteria than electron emission: biocompatibility [20, 18], commercial availabilities, production methods. To fill this gap many studies have been done using Monte-Carlo simulation methods [6, 8, 15, 14, 13, 9] with particle transport codes like Livermore-Geant4 or PENELOPE-Geant4

[1, 2, 16, 21]. These simulations are time consuming, strongly code and model dependent and do not allow the easy analysis of key parameters such size and composition. Therefore to complete these purely Monte-Carlo simulation studies, we propose a semi-analytical original approach for the electron emission of high-Z nanoparticles. This approach combines a pure analytical model for photon trajectories and an electron cascade model partly based here on Monte-Carlo Livermore-Geant4 simulations, but which can be obtained by other models.

In the first part of this paper, we develop the electron emission model for a nanoparticle and for an infinite plane surface. In a second part dedicated to discussion, we compare our model to Livermore-Geant4 results. We also compare nanoparticle and infinite plane surface electron emission and we analyse the place where electrons are produced inside nanoparticle and plane surface. Finally we analyse the influence of the nanoparticle radius on nanoparticle electron emission with our model.

2 Nanoparticle electron emission

We develop in this section the semi-analytical model for the electron emission of a spherical nanoparticle.

2.1 Photon trajectory probability

Our goal in this section is to determine the absorption probability density function (p.d.f.) of a photon in any point P of the nanoparticle. We consider the trajectory of a photon of energy E_γ incident to the nanoparticle at an entry point called M . The photon trajectory geometry is described on Fig.1. Subfigures (a) and (b) represent the (MPO) plan where O is the nanoparticle center, M is the entry point specified by the cylindrical coordinates system (r_c, φ, z_c) of origin O and local orthogonal unit vectors $(\vec{e}_{rc}, \vec{e}_\varphi, \vec{e}_z)$. P is the absorption point specified by the coordinates $(r_c, \varphi, z_c - r_\gamma)$ in the cylindrical coordinates system or by the spherical coordinates system (r_p, θ_p, φ) of origin O and local orthogonal unit vectors $(\vec{e}_{rp}, \vec{e}_{\theta p}, \vec{e}_\varphi)$. We have also represented on on Fig.1 the radius R of the nanoparticle and its surface by a blue circle. The subfigure (c) represents the nanoparticle seen in the irradiation direction i.e. \vec{e}_z direction. Considering that the irradiation source is far from the nanoparticle comparatively to its

*Electronic address: romain.casta@irsamc.ups-tlse.fr

radius R , a very good approximation is to consider parallel photon irradiation.

2.1.1 Incident and azimuthal angle probability density function (p.d.f.)

If the photon trajectories are parallel and if the photons are uniformly distributed, we can write the probability $p(M)dS_M$ that a photon goes through an infinitesimal horizontal surface $dS_M = r_c dr_c d\varphi$ around a point M as:

$$p(M)dS_M = \frac{dS_M}{\pi R^2} = \frac{r_c dr_c d\varphi}{\pi R^2} \quad (1)$$

Writing r_c as a function of θ_γ : $r_c = R \sin(\theta_\gamma)$ (see Fig.1(a)) we then have:

$$\begin{aligned} p(r_c, \varphi)r_c dr_c d\varphi &= p(\theta_\gamma, \varphi)d\theta_\gamma d\varphi \\ &= \frac{r_c}{\pi R^2} \frac{\partial r_c}{\partial \theta_\gamma} d\theta_\gamma d\varphi = \frac{\sin(2\theta_\gamma)}{2\pi} d\theta_\gamma d\varphi \end{aligned} \quad (2)$$

which is the incident and azimuthal angle p.d.f..

2.1.2 Photon path length r_γ probability density function (p.d.f.)

In this section we determine the p.d.f. that a photon goes through the nanoparticle on a distance r_γ (see Fig.1(a)) and is absorbed.

Considering the X-ray photon energy and the nanoparticle high-Z uniform composition, we choose to consider only the photo-electric interaction for photons. We assume that photons are not scattered and nor they lose their energies on their tracks except if they are completely absorbed and stopped by a photo-electric process, and emit electrons.

Following these approximations, we can write the expression of the probability that a photon goes through a distance r_γ inside the high-Z material composing the nanoparticle and reacts as:

$$p(r_\gamma)dr_\gamma = \frac{\exp(-r_\gamma/\lambda_\gamma)}{\lambda_\gamma} dr_\gamma \quad (3)$$

where λ_γ is the photon mean free path inside the nanoparticle material.

The probability that the photon goes through a path length r_γ is approximated by a classical Beer-Lambert law and the absorption probability is just $1/\lambda_\gamma$. The photon mean free path λ_γ is strongly photon energy and nanoparticle material dependent.

2.1.3 Absorption probability density function (p.d.f.)

We study the probability that a photon be absorbed in a volume dV_p around a point P of the nanoparticle. Using (2) and (3) we can write the absorption p.d.f. in the cylindrical coordinates system:

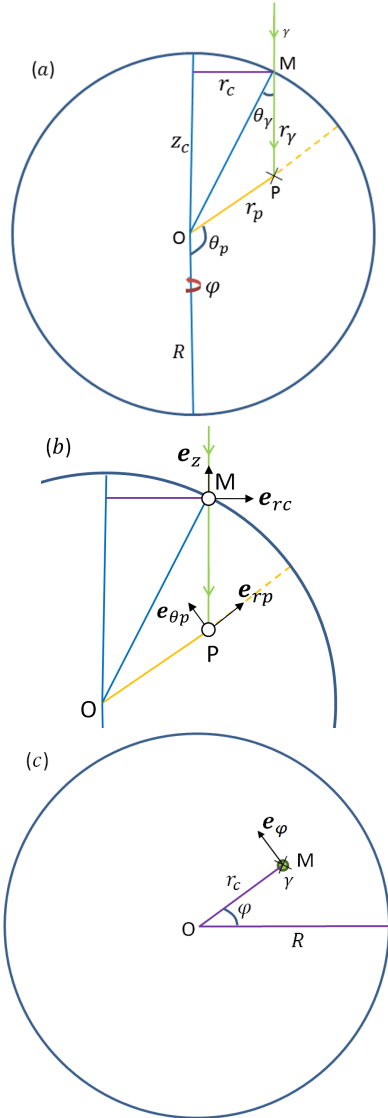


Figure 1: Photon trajectory in the plan (MPO) through the nanoparticle (a) and (b) and the nanoparticle seen in the irradiated direction (c).

$$\begin{aligned}
p(P)dV_p &= p(r_c, \varphi, z_c - r_\gamma)r_c dr_c d\varphi dz_c - r_\gamma \\
&= p(r_\gamma)p(r_c, \varphi)r_c dr_c d\varphi dr_\gamma \\
&= \frac{\exp(-r_\gamma/\lambda_\gamma) \sin(2\theta_\gamma)}{2\pi\lambda_\gamma} dr_\gamma d\theta_\gamma d\varphi \quad (4)
\end{aligned}$$

We can also express the same $p(P)dV_p$ absorption probability in the (r_p, θ_p, φ) spherical coordinate system:

$$p(P)dV_p = p(r_p, \theta_p, \varphi)r_p^2 \sin \theta_p dr_p d\theta_p d\varphi \quad (5)$$

Finally by doing the change of variables $(r_\gamma, \theta_\gamma) \rightarrow (r_p, \theta_p)$, we can express the absorption probability, as a function of (r_p, θ_p, φ) , in an infinitesimal volume dV_p around a point P of the nanoparticle.:

$$\begin{aligned}
p(r_p, \theta_p, \varphi)dV_p &= p(r_p, \theta_p, \varphi)r_p^2 \sin \theta_p dr_p d\theta_p d\varphi \\
&= \frac{\exp(-r_\gamma/\lambda_\gamma) \sin(2\theta_\gamma)}{2\pi\lambda_\gamma} \left| \frac{\partial(r_\gamma, \theta_\gamma)}{\partial(r_p, \theta_p)} \right| dr_p d\theta_p d\varphi \quad (6)
\end{aligned}$$

To complete this equation, we need to write r_γ and θ_γ as a function of r_p and θ_p :

$$\theta_\gamma = \sin^{-1} \left(\frac{r_p \sin \theta_p}{R} \right) \quad (7)$$

$$r_\gamma = \frac{R \sin(\theta_p + \theta_\gamma)}{\sin \theta_p} \quad (8)$$

Leading to the corresponding Jacobian matrix determinant which is:

$$\left| \frac{\partial(r_\gamma, \theta_\gamma)}{\partial(r_p, \theta_p)} \right| = \frac{r_p}{R \cos \theta_\gamma} \quad (9)$$

2.1.4 Application: Absorption probability density function (p.d.f.) as a function of r_p/R

It is interesting to integrate the equation (6) over θ_p in order to draw the photon absorption p.d.f. as a function of the relative distance r_p/R to the nanoparticle center. We performed this integration with a Monte Carlo numerical method, as an example, for $R = 5nm$, $E_\gamma = 1486.5eV$ and $\lambda_\gamma = 247.874nm$ (corresponding to gold material) and we draw the result on Fig.2.

To check our model results, we compare them with a Monte-Carlo particles transport simulation performed ten millions times with the Livermore Model implemented in Geant4 for the same R , E_γ , λ_γ parameters. The Livermore model (Salvat et al, 2011; Wright, 2012) includes among others photoelectric process, electrons scattering and electron impact ionization processes. In our case, this model is implemented in the transport toolkit Geant4 (Agostinelli et al, 2003; Allison et al, 2006) that we use in its 4.9.6 version.

The E_γ photon energy corresponds to the energy of a Al K_α X-ray source used in a previous work [6] where we compared experimental gold nanoparticle and gold plane surface electron emission, with Monte-Carlo simulations.

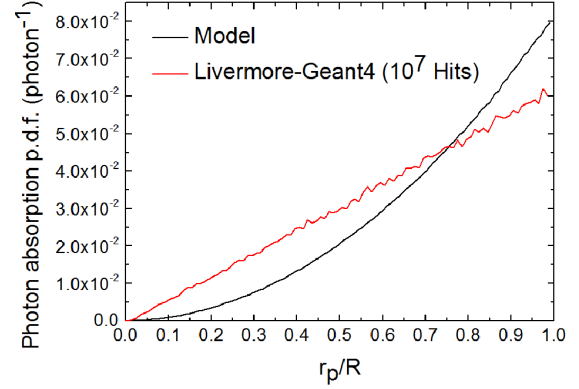


Figure 2: Absorption p.d.f. as a function of r_p/R from our model (black) and from Livermore-Geant4 (red) for a gold nanoparticle of radius $R = 5nm$ and $E_\gamma = 1486.5eV$.

We observe that the p.d.f. integral over r_p/R is not equal to 1. This is due to the small photon number absorbed (i.e. the integral over all r_p/R values) by the nanoparticle, 2.6% in our case. The two curves show a difference between our model and the Livermore-Geant4 simulation. Indeed for this last one, the p.d.f. is linear as a function of r_p/R whereas the model one follows a quadratic function. This difference is not explained for the moment but originates probably in the Geant4 nanoparticle geometry management. Nevertheless the two p.d.f. are very close which confirms our approach. The Livermore-Geant4 p.d.f. can be seen as a good approximation of the model one.

2.2 Electron cascade trajectory probability density function (p.d.f.)

At the keV energy range of interest, photon trajectories are quite simple: photons do not loose energy and are not scattered during their tracks. But their absorptions inside the nanoparticle give rise to the creation of free electrons by photo-electric processes. These primary electrons scatter inside the matter and create secondary electrons of lower energies by electron impact ionisation which in turn are scattered inside the matter and can themselves create secondary electrons. Lets call this process an electron cascade. Some of these electrons can reach the nanoparticle surface and contribute to the nanoparticle electron emission.

2.2.1 Electron cascade probability density function (p.d.f.) approximation from Livermore-Geant4 in the bulk solid

In this section we define and study the electron cascade p.d.f. in an infinite solid before including it in our nanoparticle model.

For a single absorption event, lets define at any point within the solid the electron cascade probability as the probability that an electron of energy E produced in the cascade goes through the infinitesimal surface around this point. The electron cascade

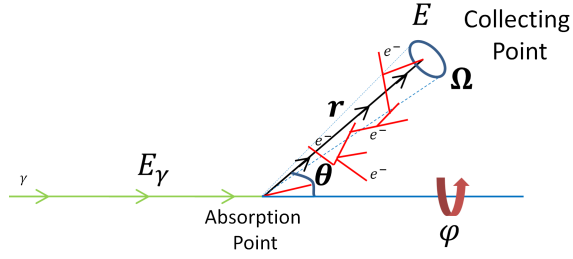


Figure 3: Electron cascade p.d.f. $\psi(E_\gamma, E, r, \theta, \phi)$ schematic geometry.

probability is given by:

$$\psi(E_\gamma, E, r, \Omega) d\Omega dE = \psi(E_\gamma, E, r, \theta, \phi) \sin\theta d\theta d\phi dE \quad (10)$$

It is the probability to find an electron of energy E in an infinitesimal solid angle $d\Omega$ after a photo-electric reaction of a photon of energy E_γ , given the distance r to the absorption point, and the photon energy E_γ as described on Fig.3.

Here we do not analytically compute the p.d.f. ψ but we approximate it from Livermore-Geant4 by simulating the experiment shown on Fig.3 fifty million times for each r value with a low cutoff at 100eV for electrons and photons. We compute energy E_e , path length r and scattering angle θ for all the electrons emitted forward i.e. the backscattered electrons are not scored and we assume that the ϕ p.d.f. follows a uniform law. From these collected data we draw a 3D histogram. We choose relatively small bin sizes: $\Delta r = 0.1nm$, $\Delta\theta = \pi/100$ and $\Delta E = 1eV$, in order to have a good approximation. Each value of the p.d.f. ψ is approximated to its corresponding bin value in the 3D histogram. The relative error is evaluated to a few percents by measuring the 3D-histogram noise intensity. The Livermore-Geant4 model reliability has been successfully confronted to the experiment (see [6]).

Fig.4 shows a few values of the approximated electron cascade p.d.f. in gold, integrated over angles θ and ϕ for $E_\gamma = 1486.5eV$. We observe that p.d.f. values are very small for $r > 28nm$ compared to smaller r values. Therefore we approximate this p.d.f. to zero for r values superior to 30nm.

On this figure, $\int \psi d\Omega$ p.d.f. shows photo-electric peaks for the small r values. They go broader as we move away from the absorption and finally merge into the electron background. These peaks are analysed in details in [6].

2.2.2 Inclusion of the electron cascade probability density function (p.d.f.) approximation into the nanoparticle model

Now that we have computed the electron cascade p.d.f. lets inject it in the nanoparticle model.

We represent the photon and electron cascade trajectories on Fig.5 where r_e is the distance from the absorption point P to a nanoparticle surface point N specified in the spherical coordinates system (r_e, θ_e, ϕ_e) of origin P and local orthogonal unit vectors $(\vec{e}_{r_e}, \vec{e}_{\theta_e}, \vec{e}_{\phi_e})$.

We can associate the electron cascade p.d.f. defined in (10) to the electron cascade trajectory PN . We write the probability

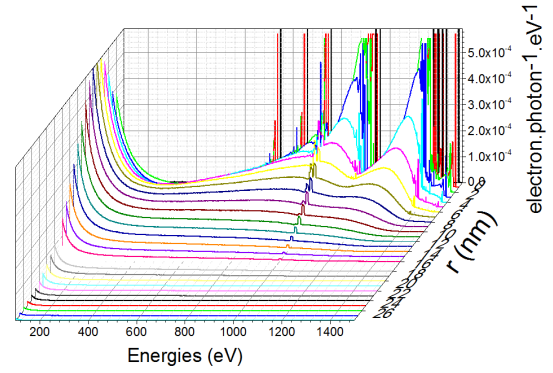


Figure 4: Electron cascade p.d.f. in gold for $E_\gamma = 1486.7eV$ integrated over angles i.e. $\int \psi(E_\gamma, E, r, \Omega) d\Omega$ for $1nm \leq r \leq 28nm$ and $150eV \leq E \leq 1500eV$.

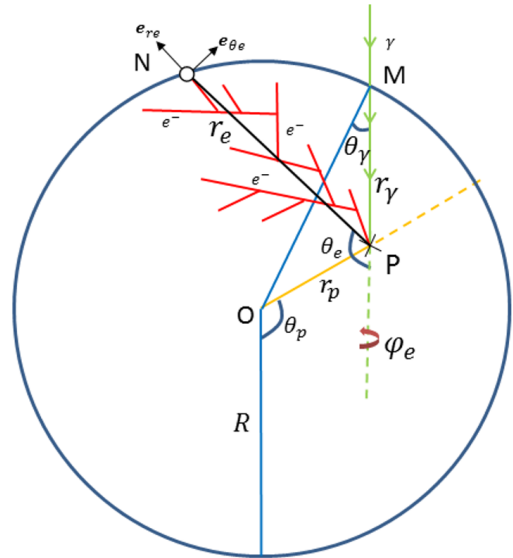


Figure 5: Photon and electron cascade trajectories in a particular cross-section.

to find an electron of energy E_e in the infinitesimal solid angle $d\Omega_e = \sin\theta_e d\theta_e d\varphi_e$ around $N(r_e, \theta_e, \varphi_e)$ given the length r_e between the photon absorption point P and the surface point N , and the photon energy E_γ :

$$\psi(E_\gamma, E_e, r_e, \theta_e, \varphi_e) \sin\theta_e d\theta_e d\varphi_e dE_e \quad (11)$$

2.3 Electron emission probability density function (p.d.f.)

We can multiply photon absorption and electron cascade p.d.f. in order to obtain the probability of an incident photon entering in the nanoparticle at M , absorbed at P and producing an electron cascade ejecting an electron of energy E_e at a surface point N :

$$\frac{e^{-r_\gamma/\lambda_\gamma} \sin(2\theta_\gamma)}{2\pi\lambda_\gamma} \left| \frac{\partial(r_\gamma, \theta_\gamma)}{\partial(r_p, \theta_p)} \right| dr_p d\theta_p d\varphi \quad (12)$$

$$\times \psi(E_\gamma, E_e, r_e, \theta_e, \varphi_e) \sin\theta_e d\theta_e d\varphi_e dE_e$$

r_e can be written as a function of the integration variables:

$$r_e = -r_p(\cos\varphi_e \sin\theta_e \sin\theta_p + \cos\theta_e \cos\theta_p) + \sqrt{\begin{pmatrix} \cos^2\varphi_e \sin^2\theta_e \sin^2\theta_p \\ + 0.5 \cos\varphi_e \sin(2\theta_e) \sin(2\theta_p) \\ + \cos^2\theta_e \cos^2\theta_p - 1 \end{pmatrix}} + R^2 \quad (13)$$

We can integrate (12) over the variables (r_p, θ_p, φ) and (θ_e, φ_e) corresponding respectively to the absorption points P and the surface points N . Hence we get the total nanoparticle electron emission at an energy E_e :

$$p(E_e) dE_e = \left(\int_P \int_N \frac{e^{-r_\gamma/\lambda_\gamma} \sin(2\theta_\gamma)}{2\pi\lambda_\gamma} \left| \frac{\partial(r_\gamma, \theta_\gamma)}{\partial(r_p, \theta_p)} \right| \times \psi(E_\gamma, E_e, r_e, \theta_e, \varphi_e) \sin\theta_e d\theta_e d\varphi_e d\theta_p d\varphi dr_p \right) dE_e \quad (14)$$

By replacing $\psi(E_\gamma, E_e, r_e, \theta_e, \varphi_e)$ by its Livermore-Geant4 approximation, we can numerically compute this integral with a Monte-Carlo method. We do it on a large range of energies and we draw the resulting electron emission intensity as a function of the electron energies.

The obtained spectrum is shown on Fig.6 for a X-ray energy value of $E_\gamma = 1486.5eV$ and a gold nanoparticle of $R = 5nm$ as an example. It is compared with a purely Livermore-Geant4 simulation of ten millions hits, with the same parameters. The computing times comparison is clearly at the advantage of the model. For the same relative standard deviation, it takes $38min$ to compute the whole electron emission spectrum with the Livermore-Geant4 model whereas it takes only $90s$ with our model. This gain in time can be largely improved by refining the integration method. The computations were performed on a computer equipped with an Intel Core i7-3770 processor and 16GB memory.

We can see that both spectra are very close but present a few differences which are explained by the photon absorption p.d.f. (Fig.2) in a following section.

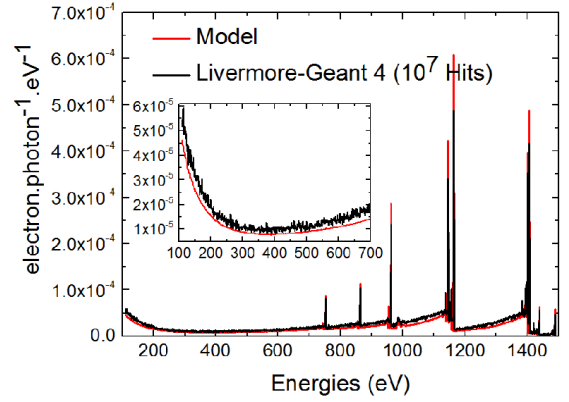


Figure 6: Model and Livermore-Geant4 electron emission spectra for a gold nanoparticle, $R = 5nm$ and $E_\gamma = 1486.5eV$. The spectra are zoomed to the range $100eV - 700eV$ in the upper box.

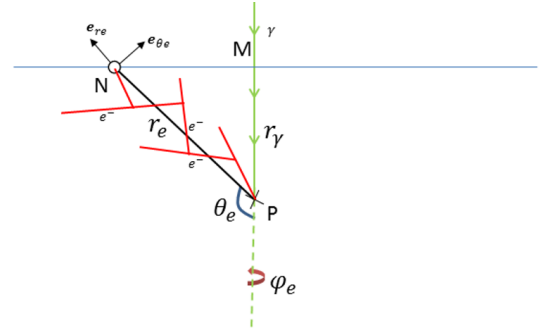


Figure 7: Infinite plane surface photon and electron trajectories.

Our model is reliable as long as the photo-electric process is the main photo-reaction process of photons inside the nanoparticle material. The electron trajectory reliability is fully dependent of the model used. In the Livermore-Geant4 case, we assume that the electron trajectory simulations are correct until $100eV$. In our specific case, the model is valid in the photon energy range $100eV - 1MeV$, and for electron of energies higher than $100eV$. This work can be achieved for higher photon energy used in radiotherapy treatment with the same method and with the Livermore-Geant4 model for example. This will be the subject of a next paper.

3 Plane surface electron emission

In a previous paper [6], we compared nanoparticle of radius $19nm$ and very large gold plane surface experimental electron emission spectra. To complete this work, we have decided to develop this model for plane surface electron emission too.

As well as for nanoparticles we consider the photon and the electron cascade trajectories. These are represented on Fig.7. M is the entry point, P the absorption point specified by its depth r_γ and N the exit point specified by the spherical coordinates system $(r_e, \theta_e, \varphi_e)$ of origin P and local orthogonal unit vectors $(\vec{e}_{re}, \vec{e}_{\theta_e}, \vec{e}_{\varphi_e})$.

In the same approximations than for nanoparticles and by integrating over all the surface points $N(\theta_e, \varphi_e)$ and the depth r_γ , we

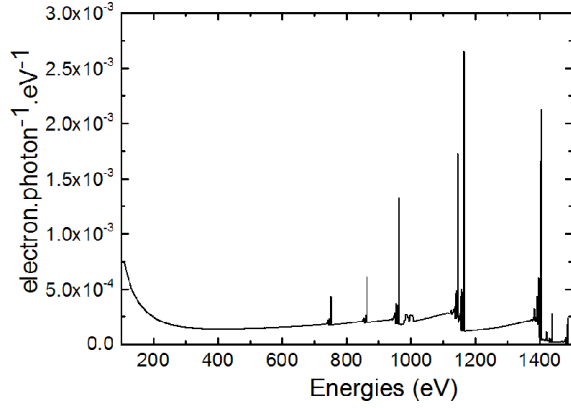


Figure 8: Electron emission spectrum for a gold plane surface.

express the total infinite plane surface electron emission p.d.f. for an energy E_e as:

$$p(E_e)dE_e = \left(\int_{\pi/2}^{\pi} \int_0^{\infty} \frac{e^{-r_\gamma/\lambda_\gamma}}{\lambda_\gamma} \times 2\pi\psi(E_\gamma, E_e, r_e, \theta_e, \varphi_e) \sin\theta_e dr_\gamma d\theta_e \right) dE_e \quad (15)$$

Again we have r_e as a function of r_γ and θ_e :

$$r_e = -\frac{r_\gamma}{\cos\theta_e} \quad (16)$$

We integrate this p.d.f. by a Monte-Carlo numerical method for a gold plane surface as an example. The result is shown on Fig.8.

We can see that the electron emission for the plane surface is much larger than for the 5nm radius nanoparticle (Fig.6). For example the surface electron emissions are 1.38×10^{-4} *electron.photon*⁻¹.*eV*⁻¹ at 400eV and 2.65×10^{-3} *electron.photon*⁻¹.*eV*⁻¹ at 1164eV whereas for the nanoparticle the electron emissions are respectively 8.07×10^{-6} and 6.09×10^{-4} . This is explained by the larger photon number absorbed by the gold surface plane than by the gold nanoparticle.

Indeed, because of its infinite depth all the incident photons are absorbed by the plane surface, producing photo-electrons whereas only 2.6% of the incident photons are absorbed by the nanoparticle of radius 5nm. We do a more extensive comparison in a further section.

4 Discussion

4.1 Nanoparticle electron cascade production depth

Before going further, we choose to study the electron cascade production depth p.d.f.. To obtain this p.d.f., we numerically integrate equation (12) on all the variables excepted r_p and E_e and draw the resulting p.d.f. which represents the electron cascade production depth i.e. the probability that a photon of energy E_γ reacts at a distance r_p from the nanoparticle center and produces an electron of energy E_e at the nanoparticle surface. We draw

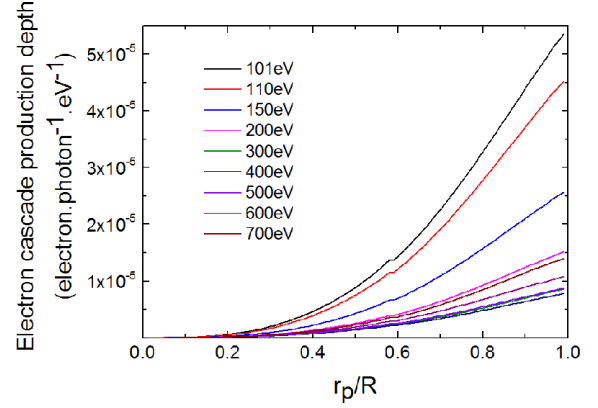


Figure 9: Electron cascade production depth p.d.f. i.e. p.d.f. that a photon of energy E_γ reacts at a distance r_p from the gold nanoparticle center and produces an electron of energy E_e at the nanoparticle surface as a function of r_p/R , for $R = 5nm$ and $E_\gamma = 1486.5eV$.

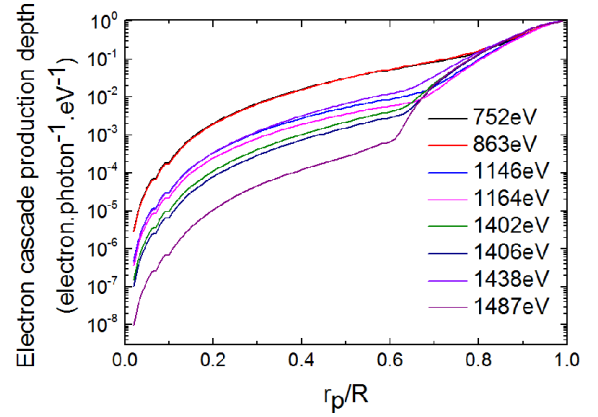


Figure 10: P.d.f. that a photon of energy $E_\gamma = 1486.5eV$ reacts at a distance r_p , from the center of a gold nanoparticle of radius $R = 5nm$, and produces an electron of energy E_e at the nanoparticle surface as a function of r_p/R for photo-electric lines.

it on Fig.9 for a gold nanoparticle of radius 5nm irradiated by 1486.5eV photons, and few electrons energies located in the electron background range 100eV – 700eV.

These electron cascade production depth p.d.f. show, as expected, that most of the emitted electrons are produced by absorption close from the nanoparticle surface. After normalization we notice that all of them follow the same non-linear function which has a maximum at the nanoparticle surface.

This non-linear function is not completely described by the electron cascade production depth p.d.f. of the photo-electric peak energies as we see on Fig.10.

Indeed, the previous p.d.f. is constituted of secondary electrons forming the peaks bases and the electron background. The production depth p.d.f. of the primary photo-electrons, ejected at the nanoparticle surface constituting most of the photo-electric peaks are created directly by photons shallower in the nanoparticle. That is why for the peak energies, their production depth p.d.f. are the same than the electron background p.d.f. until $r_p/R = 0.5$ then diverge more and more till $r_p/R = 1$.

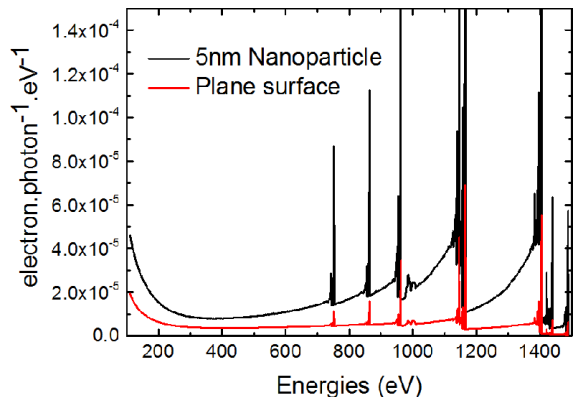


Figure 11: Electron emission spectra normalized to the absorbed photon number for a gold infinite plane surface and a gold nanoparticle of radius $5nm$ irradiated perpendicularly by $1486.5eV$ photons.

4.2 Comparison between our model and Livermore-Geant4

From the spectra shown on Fig.6 we see that our model results are consistent with the Livermore-Geant4 ones. But both spectra do not exactly match. The model continuous background is slightly below the Livermore-Geant4 one and the model photo-electric peak intensities are above the Livermore-Geant4 ones as seen on Tab.1.

These differences are explained by the photon absorption p.d.f.. We observe on Fig.2 that these p.d.f. are comparable but slightly different. As seen before, the Livermore-Geant4 curve follows a linear function with the relative distance r_p/R to the nanoparticle center whereas the model one follows a non-linear quadratic function. As a consequence the model absorption probability is larger than the Livermore-Geant4 one under $0.75R$ and smaller over these values.

However as we have seen on Fig.10, the surface nanoparticle (where model photon absorption p.d.f. is larger) is the production place of the photo-electric line electrons. So the gap between the model and the Livermore-Geant4 photo-electric line intensities presented on Tab.1 is due to the difference between the photon absorption p.d.f. after $0.75R$. By the same way the gap between electron background is explained by the difference between photon absorption p.d.f. before $0.75R$.

4.3 Comparison between model nanoparticle and plane surface electron emission

To compare a gold nanoparticle of radius $5nm$ and a gold infinite plane surface electron emission, we normalize both spectra by the number of absorbed photons. The results are presented on Fig.11 for electron emission spectra and on Tab.2 for photo-electric line intensities.

We can see that the number of emitted electrons by photon absorption is much greater for the nanoparticle than for the gold plane surface. This is due to the small nanoparticle size. Indeed each photon absorbed by the nanoparticle produces an electron cascade which as seen on Fig.2 is at a distance of a few nanometers of the nanoparticle surface. So there is a high probability that

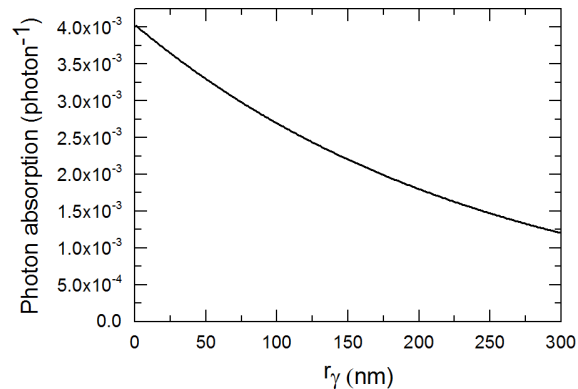


Figure 12: Photon absorption p.d.f. for a gold infinite plane surface as a function of r_γ from our model.

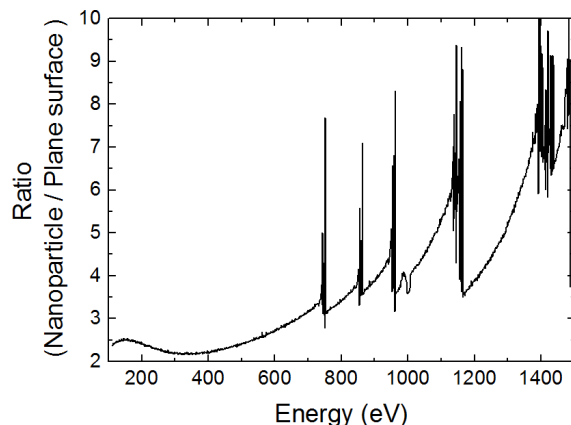


Figure 13: Ratio between gold nanoparticle of radius $5nm$ and infinite gold plane surface electron emission.

this cascade creates electrons at the nanoparticle surface.

As seen in Fig.12, in the infinite plane surface, all the photons are absorbed but for most of them this happens too deep from the surface to create electron cascades which have a reasonable chance to reach the surface. Indeed by observing the electron cascade $\int \psi d\Omega$ p.d.f. on Fig.4, we see that after $30nm$ there is almost no chance for these electrons to reach the surface.

In order to compare in details both normalized electron emission, we draw their ratios i.e. we divide the $5nm$ radius gold nanoparticle electron emission spectra intensity by the corresponding gold plane surface intensity. The resulting ratio is presented on Fig.13 for spectra and on Tab.2 for photo-electric line intensities.

We observe on Tab.2 that the photo-electric line intensities normalized to the absorbed photon number are much larger (between 7 and 10 times) for nanoparticle than for the plane surface. We also observe on the spectra ratio Fig.13 that after each peak the ratio slowly decreases, as a consequence of the electron cascade p.d.f. $\int \psi d\Omega$.

We present this p.d.f. $\int \psi d\Omega$ as a function of the distance r from absorption point, for energies between $1110eV$ and $1010eV$ on Fig.14. We see that the further we move down from the peak energy ($1146eV$ in our case), the lower are the probabilities to find an electron at a small distance from the absorption point (Fig.14(b)). On the other hand, as we move down from the peak

Energies <i>eV</i>	Model <i>electron.photon⁻¹.eV⁻¹</i>	Livermore-Geant4 <i>electron.photon⁻¹.eV⁻¹</i>	Ratios
752	6.34×10^{-5}	7.26×10^{-5}	1.15
863	8.26×10^{-5}	9.40×10^{-5}	1.14
962	2.71×10^{-4}	2.19×10^{-4}	0.81
1146	3.94×10^{-4}	3.06×10^{-4}	0.78
1164	5.98×10^{-4}	4.72×10^{-4}	0.79
1402	3.18×10^{-4}	3.25×10^{-4}	1.02
1406	4.83×10^{-4}	4.10×10^{-4}	0.85
1438	6.02×10^{-5}	4.98×10^{-5}	0.83
1489	5.72×10^{-5}	4.65×10^{-5}	0.81

Table 1: Model and Livermore-Geant4 photo-electric line intensities from the baselines have been subtracted and their ratios for $5nm$ radius gold nanoparticle and $E_\gamma = 1486.5eV$.

Energies <i>eV</i>	5nm Nanoparticle <i>electron.photon⁻¹.eV⁻¹</i>	Plane Surface <i>electron.photon⁻¹.eV⁻¹</i>	Ratios
752	7.26×10^{-5}	6.74×10^{-6}	10.77
863	9.40×10^{-5}	1.08×10^{-5}	8.73
962	2.19×10^{-4}	3.00×10^{-5}	7.31
1146	3.06×10^{-4}	3.99×10^{-5}	7.66
1164	4.72×10^{-4}	6.59×10^{-5}	7.15
1402	3.25×10^{-4}	3.36×10^{-5}	9.66
1406	4.11×10^{-4}	5.44×10^{-5}	7.55
1438	4.98×10^{-5}	6.63×10^{-5}	7.52
1489	4.65×10^{-5}	6.32×10^{-5}	7.36

Table 2: Photo-electric line intensities from the baselines have been subtracted and their ratios, normalized to the number of absorbed photon, for a $5nm$ radius gold nanoparticle and an infinite gold plane surface with $E_\gamma = 1486.5eV$.

energy we observe an increase of the $\int \psi d\Omega$ p.d.f. for r values between $3.5nm$ and $7nm$ (Fig.14(c)) and there is clearly a shift of $\int \psi d\Omega$ maximum to larger r values (Fig.14(a)).

In a $5nm$ radius nanoparticle, we know that most of the absorption points are close from the surface ($< 3nm$). Consequently, the nanoparticle electron emission is strongly affected by the decrease of $\int \psi d\Omega$ p.d.f. at small r values. The plane surface absorptions are located as seen previously further from the surface and are less affected by this decrease.

For these reasons, as we move down from the peak energy, there is a stronger decrease for nanoparticle electron intensities than for plane surfaces, explaining the ratio decrease between both electron emissions.

4.4 Radius impact on nanoparticle electron emission

One of the main interest of our model is that we can keep the same electron cascade p.d.f. but easily change the nanoparticle radius, which is a critical parameter. This is an important gain of computing time compared to a full Monte-Carlo simulation approach classically used. To study the radius influence over the electron emission, we compute it for several radii from $1nm$ to $100nm$ and present few of them on Fig.15. We observe that the electron emission rapidly increases from $1nm$ to $15nm$ and then saturates. The spectrum form does not seem to depend of the nanoparticle radius.

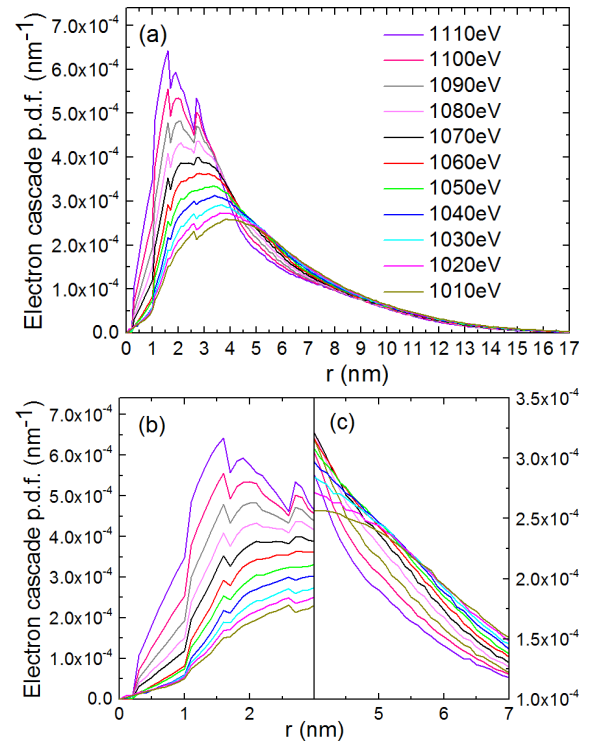


Figure 14: Electron cascade p.d.f. integrated over solid angle $\int \psi d\Omega$ for gold, $1010eV < E_e < 1110eV$, and $E_\gamma = 1486.5eV$ for range $0 - 17nm$ (a), $0 - 3nm$ (b) and $4 - 7nm$ (c).

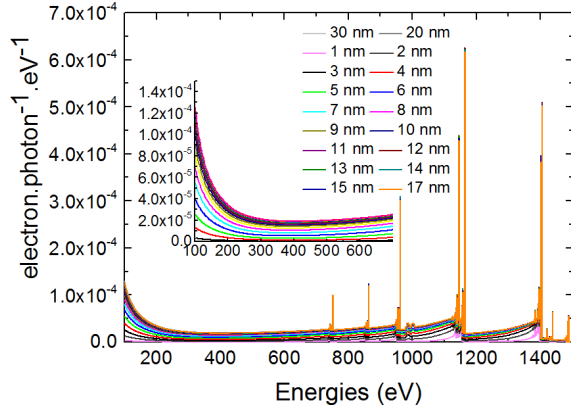


Figure 15: Gold nanoparticle electron emission spectra computed with the previous developed model for different nanoparticle radii.

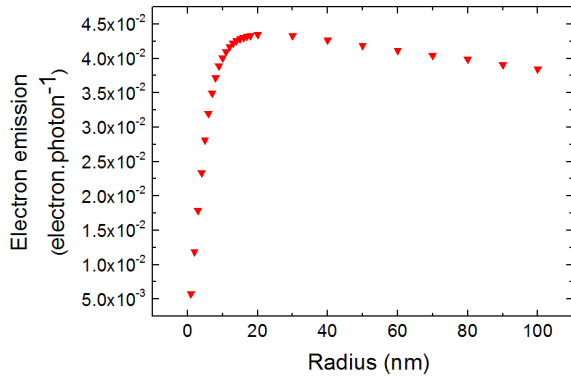


Figure 16: Total gold nanoparticle electron emission computed with the developed model for different nanoparticle radii.

To have a more accurate information about the radius influence, we draw the nanoparticle electron emission integrated over the ejected electrons energy E_e from $100eV$ to $1500eV$ as a function of the nanoparticle radius on Fig.16. We see, as expected, an important increase from $1nm$ to $15nm$ and then a slow decrease.

These features can be explained qualitatively by the total photon absorption p.d.f. as a function of nanoparticle radius, shown on Fig.17, and by the gold electron cascade p.d.f.

$$\int_{100eV}^{1500eV} \int \psi(E_\gamma, E, r, \Omega) d\Omega dE \text{ (Fig.18)}$$

i.e. the p.d.f. that an electron cascade produces an electron at a distance r of its production place.

The total photon absorption (Fig.17) shows an increase with the nanoparticle radius, which in turn causes an increase in the first part of the total electron emission (Fig.16). Indeed if there are more photon absorbed, there are more photo-electrons produced, more electron cascades and consequently more electrons ejected at the surface.

This increase of the total electron emission stops at a maximum located at $R = 20nm$. Further a slow decrease appears because the number of electron cascades able to reach the surface is less and less important. As seen on Fig.18, once the distance from the absorption point is larger than $6nm$ the further an electron cascade is created from the absorption point, the lower its probability to reach the surface and eject electrons.

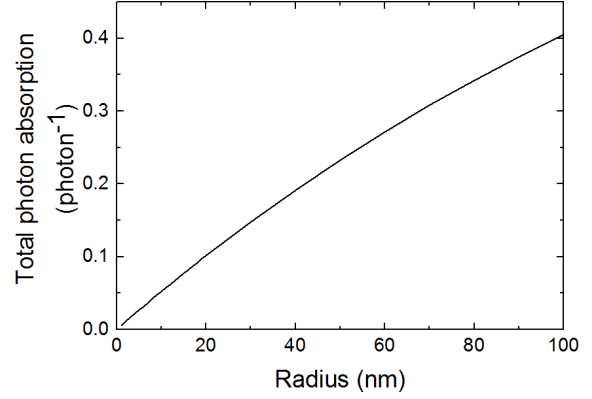


Figure 17: Total gold nanoparticle photon absorption computed with the developed model for different nanoparticle radii.

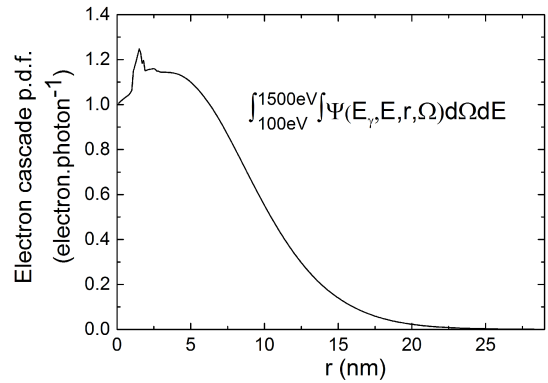


Figure 18: Gold electron cascade p.d.f. integrated over electron energy E from $100eV$ to $1500eV$ and solid angle of collection Ω

Up to $6nm$ as long as the electron emission increases, the total electron emission curve of Fig.16 follows the total absorption increase, because it is not counterbalanced by the decrease of the electron cascade p.d.f.. In small nanoparticles most of the electron cascade production points are closer than $6nm$ from the surface. As a consequence their probability to reach the surface is roughly stable as shown by Fig.18. For larger nanoparticles, the number of electron production points further than $6nm$ from the surface becomes significant and the absorption increase is counterbalanced by the decrease of the electron cascade p.d.f..

5 Conclusion

We developed an original model for the electron emission of high-Z nanoparticle and plane surface irradiated by X-ray photons. After checking that this model is compatible with the Livermore model implemented in Geant4, we used it to study the electron emission of a gold nanoparticle irradiated by $1486.5eV$ photons. This model allowed us to deeply understand key features and parameters of nanoparticle electron emission: nanoparticle size, difference between nanoparticle and plane surface electron emission, electron cascade production depth, incident photon energy. This work highlights the existence of a nanoparticle radius corresponding to a maximum electron emission. This model can be simplified by doing approximations and other electron cascade models can be included. It can be checked with other simulation codes, photon energies or nanoparticle compositions.

References

- Research Section A: Accelerators, Spectrometers, Detectors and Associated Equipment 506(3):250 – 303
- [1] Agostinelli S, Allison J, Amako K, Apostolakis J, Araujo H, Arce P, Asai M, Axen D, Banerjee S, Barrand G, Behner F, Bellagamba L, Boudreau J, Broglia L, Brunengo A, Burkhardt H, Chauvie S, Chuma J, Chytracsek R, Cooperman G, Cosmo G, Degtyarenko P, Dell'Acqua A, Depaola G, Dietrich D, Enami R, Feliciello A, Ferguson C, Fesefeldt H, Folger G, Foppiano F, Forti A, Garelli S, Giani S, Giannitrapani R, Gibin D, Cadenas JG, Gonzalez I, Abril GG, Greeniaus G, Greiner W, Grichine V, Grossheim A, Guatelli S, Gumplinger P, Hamatsu R, Hashimoto K, Hasegawa H, Heikkinen A, Howard A, Ivanchenko V, Johnson A, Jones F, Kallenbach J, Kanaya N, Kawabata M, Kawabata Y, Kawaguti M, Kelner S, Kent P, Kimura A, Kodama T, Kokoulin R, Kossov M, Kurashige H, Lamanna E, Lampert T, Lara V, Lefebvre V, Lei F, Liendl M, Lockman W, Longo F, Magni S, Maire M, Medernach E, Minamimoto K, de Freitas PM, Morita Y, Murakami K, Nagamatsu M, Nartallo R, Nieminen P, Nishimura T, Ohtsubo K, Okamura M, O'Neale S, Oohata Y, Paech K, Perl J, Pfeiffer A, Pia M, Ranjard F, Rybin A, Sadilov S, Salvo ED, Santin G, Sasaki T, Savvas N, Sawada Y, Scherer S, Sei S, Sirotenko V, Smith D, Starkov N, Stoecker H, Sulkimo J, Takahata M, Tanaka S, Tcherniaev E, Tehrani ES, Tropeano M, Truscott P, Uno H, Urban L, Urban P, Verderi M, Walkden A, Wander W, Weber H, Wellisch J, Wenaus T, Williams D, Wright D, Yamada T, Yoshida H, Zschiesche D (2003) Geant4 a simulation toolkit. *Nuclear Instruments and Methods in Physics Research Section A: Accelerators, Spectrometers, Detectors and Associated Equipment* 506(3):250 – 303
 - [2] Allison J, Amako K, Apostolakis J, Araujo H, Dubois P, Asai M, Barrand G, Capra R, Chauvie S, Chytracsek R, Cirrone GAP, Cooperman G, Cosmo G, Cuttone G, Daquino GG, Donszelmann M, Dressel M, Folger G, Foppiano F, Generowicz J, Grichine V, Guatelli S, Gumplinger P, Heikkinen A, Hrivnacova I, Howard A, Incerti S, Ivanchenko V, Johnson T, Jones F, Koi T, Kokoulin R, Kossov M, Kurashige H, Lara V, Larsson S, Lei F, Link O, Longo F, Maire M, Mantero A, Mascialino B, McLaren I, Lorenzo P, Minamimoto K, Murakami K, Nieminen P, Pandola L, Parlati S, Peralta L, Perl J, Pfeiffer A, Pia M, Ribon A, Rodrigues P, Russo G, Sadilov S, Santin G, Sasaki T, Smith D, Starkov N, Tanaka S, Tcherniaev E, Tome B, Trindade A, Truscott P, Urban L, Verderi M, Walkden A, Wellisch JP, Williams D, Wright D, Yoshida H (2006) Geant4 developments and applications. *Nuclear Science, IEEE Transactions on* 53(1):270–278
 - [3] Brun E, Cloutier P, Sicard-Roselli C, Fromm M, Sanchez L (2009) Damage induced to dna by low-energy (0-30 eV) electrons under vacuum and atmospheric conditions. *Journal of Physical Chemistry B* 113(29):10,008–10,013
 - [4] Butterworth KT, Wyer JA, Brennan-Fournet M, Latimer CJ, Shah MB, Currell FJ, Hirst DG (2008) Variation of strand break yield for plasmid dna irradiated with high-z metal nanoparticles. *Radiation Research* 170(3):381–387
 - [5] Carter JD, Cheng NN, Qu Y, Suarez GD, Guo T (2007) Nanoscale energy deposition by x-ray absorbing nanostructures. *Journal of Physical Chemistry B* 111(40):11,622–11,625
 - [6] Casta R, Champeaux JP, Sence M, Moretto-Capelle P, Caffarelli P, Amsellem A, Sicard-Roselli C (2014) Electronic emission of radio-sensitizing gold nanoparticles under x-ray irradiation : experiment and simulations. *Journal of Nanoparticle Research* 16(4):2348
 - [7] Chithrani DB, Jelveh S, Jalali F, van Prooijen M, Allen C, Bristow RG, Hill RP, Jaffray DA (2010) Gold nanoparticles as radiation sensitizers in cancer therapy. *Radiation Research* 173(6):719–728
 - [8] Chow JCL, Leung MKK, A JD (2012) Monte Carlo simulation on a gold nanoparticle irradiated by electron beams. *Phys Med Biol* 57:3323–3331
 - [9] Garnica-Garza H (2013) Microdosimetry of x-ray irradiated gold nanoparticles. *Radiation Protection Dosimetry* 155:59–63
 - [10] Hainfeld JF, Slatkin DN, Smilowitz HM (2004) The use of gold nanoparticles to enhance radiotherapy in mice. *Physics in Medicine and Biology* 49
 - [11] Herold D, Das I, Stobbe C, Iyer R, Chapman J (2000) Gold microspheres: a selective technique for producing biologically effective dose enhancement. *International Journal of Radiation Biology* 76(10):1357–1364

- [12] Kennedy LC, Bickford LR, Lewinski NA, Coughlin AJ, Hu Y, Day ES, West JL (2011) A new era for cancer treatment: Gold-nanoparticle-mediated thermal therapies. *Small* 17:169–183
- [13] Lechtman E, Chattopadhyay N, Cai Z, Mashouf S, Reilly R, Pignol JP (2011) Implications on clinical scenario of gold nanoparticle radiosensitization in regards to photon energy, nanoparticle size, concentration and location. *Physics in Medicine and Biology* 56(15):4631–4647
- [14] Lechtman E, Mashouf S, Chattopadhyay N, Keller B, Lai P, Cai Z, Reilly R, J-P P (2013) A Monte Carlo-based model of gold nanoparticle radiosensitization accounting for increased radiobiological effectiveness. *Phys Med Biol* 58:3075–3087
- [15] McMahon SJ, Hyland WB, Muir MF, Coulter JA, Jain S, Butterworth KT, Schettino G, Dickson GR, Hounsell AR, O’Sullivan JM, Prise KM, Hirst DG, Currell FJ (2011) Biological consequences of nanoscale energy deposition near irradiated heavy atom nanoparticles. *SCIENTIFIC REPORTS* 1
- [16] Salvat F, Fernández-Varea JM, Sempau J (2011) Penelope-2011: A code system for Monte Carlo simulation for electron and photon transport, <https://www.oecd-neo.org/science/docs/2011/nsc-doc2011-5.pdf>
- [17] Sanche L (2009) Role of secondary low energy electrons in radiobiology and chemoradiation therapy of cancer. *Chemical Physics Letters* 474:1–6
- [18] Schaeublin NM, Braydich-Stolle LK, Schrand AM, Miller JM, Hutchison J, Schlager JJ, Hussain SM (2011) Surface charge of gold nanoparticles mediates mechanism of toxicity. *Nanoscale* 3:410
- [19] Sharma R, Chen CJ (2009) Newer nanoparticles in hyperthermia treatment and thermometry. *Journal of Nanoparticle Research* 11(3):671–689
- [20] Vujacic A, Vodnik V, Joksic G, Petrovic S, Leskovac A, Nastasijevic B, Vasic V (2011) Particle size and concentration dependent cytotoxicity of citrate capped gold nanoparticles. *Digest Journal of Nanomaterials and Biostructures* 6(3):1367–1376
- [21] Wright D (2012) Geant4 10.0 - Physics reference manual, <http://geant4.web.cern.ch/geant4/UserDocumentation/UsersGuides/PhysicsReferenceManual/fo/PhysicsReferenceManual.pdf>